

Impact of contact inhibition on collective cell migration and proliferation

H. P. Jain ¹, D. Wenzel ¹ and A. Voigt ^{1,2,3}

¹*Institute of Scientific Computing, Technische Universität Dresden, D-01062 Dresden, Germany*

²*Center for Systems Biology Dresden (CSBD), Pfotenhauerstr. 108, D-01307 Dresden, Germany*

³*Cluster of Excellence - Physics of Life, TU Dresden, D-01062 Dresden, Germany*



(Received 11 August 2021; accepted 9 February 2022; published 7 March 2022)

Contact inhibition limits migration and proliferation of cells in cell colonies. We consider a multiphase field model to investigate the growth dynamics of a cell colony, composed of proliferating cells. The model takes into account the mechanism of contact inhibition of proliferation by local mechanical interactions. We compare nonmigrating and migrating cells, in order to provide a quantitative characterization of the dynamics and analyze the velocity of the colony boundary for both cases. Additionally, we measure single cell velocities, number of neighbor distributions, as well as the influence of stress and age on positions of the cells and with respect to each other.

DOI: [10.1103/PhysRevE.105.034402](https://doi.org/10.1103/PhysRevE.105.034402)

I. INTRODUCTION

Collective cell migration and proliferation play fundamental roles in embryonic development, tissue regeneration, wound healing, and many disease processes. Identifying the principles behind these processes requires a multiscale approach, linking the properties of individual cells and cell-cell interactions to the emerging collective behavior. Various modeling approaches have been considered to address this task; see [1–3] for reviews. We here use a multiphase field model (see [4–12]), which allows for cell deformations and detailed cell-cell interactions, as well as subcellular details to resolve the mechanochemical interactions underlying cell migration. Also topological changes, such as T1 transitions, follow naturally in this framework. Multiphase field models, together with efficient numerics and appropriate computing power, allow one to analyze the connection of single cell behavior with collective migration and growth of cell colonies, at least for moderate numbers of cells. They already led to quantitative predictions of many generic features in multicellular systems [12–14].

Here, we especially focus on the complex interaction of migration and proliferation, which are regulated by contact inhibition processes. We distinguish between two different inhibitory mechanisms. On the one hand, contact inhibition by locomotion (CIL), which is a process whereby a cell ceases motility or changes its trajectory upon collision with another cell by active regulation (see [15] for a review). On the other hand, contact inhibition of proliferation (CIP), which refers to the suppression of cell growth and divisions in dense regions of tissues [16,17]. CIL naturally results from mechanical interactions and re-polarization mechanisms of the multiphase field models and its impact on collective migration is well explored, within this framework [5,8–10,12,13,18,19]. However, in order to focus on CIP, we here consider a simpler motility mechanism which ignores the active regulation of

cell motility. Proliferation cannot easily be incorporated in the energetic description of a multiphase field model. Even if such attempts on a single cell level exist [20,21], we here follow an *ad hoc* procedure, which simply divides a cell if it has reached a certain size [4,22–24]. CIP is included by a growth factor for each cell, which is affected by cell-cell interactions. We study CIP for the dynamics of small groups of cells, proliferating in a circular confinement, similar to the experiments on monolayers of epithelia cells in [25,26]. In particular, we analyze emerging features, such as the speed of colony growth, the velocity of individual cells, topological measures, such as number of neighbor distributions, as well as relations between mechanical interactions and age on position of the cells in the colony. For other computational studies on CIP, but with much stronger restrictions on the deformation of cells, we refer to [24,25,27,28]. Figure 1 shows the dynamics of a growing colony for nonmigrating and migrating cells, already indicating the differences of the models with respect to morphology and velocity of the colony boundary.

The paper is structured as follows: We introduce the mathematical model in Sec. II, briefly describe the considered numerical approach to solve it in Sec. III, discuss results in Sec. IV, and draw conclusions in Sec. V. Technical details are provided in Appendixes A–E. Movies corresponding to Fig. 1 are provided in the Supplemental Material [29].

II. MODELING

We consider two-dimensional phase field variables $\phi_i(\mathbf{x}, t)$, one for each cell. Values of $\phi_i = 1$ and $\phi_i = -1$ denote the interior and the exterior of a cell, respectively. The cell boundary is defined implicitly by the region $-1 < \phi_i < 1$. The dynamics for each ϕ_i is considered as

$$\partial_t \phi_i + v_0(\mathbf{v}_i \cdot \nabla \phi_i) = \Delta \frac{\delta \mathcal{F}}{\delta \phi_i} + k_i(\phi_i + 1), \quad (1)$$

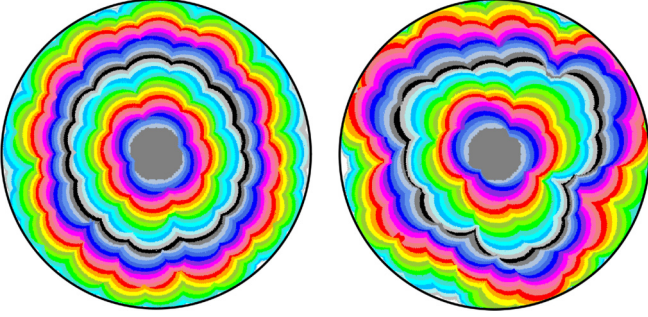


FIG. 1. Superimposed snapshots of cell colony at different times, starting with one circular cell in the center (on top, gray). (Left) nonmigrating; (right) migrating cells. The outer circle marks the confinement. For selected snapshots, also showing the individual cells of the colony, and the considered parameters, see Appendix E. For the corresponding movies see the Supplemental Material [29].

for $i = 1, \dots, N$, where $N = N(t)$ denotes the number of active cells. \mathcal{F} is a free energy and \mathbf{v}_i is a vector field used to incorporate active components, with a self-propulsion strength v_0 . For nonmigrating cells we set $v_0 = 0$. All quantities are nondimensional quantities. As in previous studies [10,12,18,30,31] we consider conserved dynamics but now add an exponential growth term with a growth rate k_i . The free energy $\mathcal{F} = \mathcal{F}_{\text{CH}} + \mathcal{F}_{\text{INT}} + \mathcal{F}_{\text{CON}}$ contains passive contributions, where

$$\mathcal{F}_{\text{CH}} = \sum_{i=1}^N \frac{1}{\text{Ca}} \int_{\Omega} \frac{\epsilon}{2} \|\nabla \phi_i\|^2 + \frac{1}{\epsilon} W(\phi_i) d\mathbf{x}, \quad (2)$$

$$\mathcal{F}_{\text{INT}} = \sum_{i=1}^N \frac{1}{\text{In}} \int_{\Omega} B(\phi_i) \sum_{j \neq i} w(\phi_j) d\mathbf{x}, \quad (3)$$

$$\mathcal{F}_{\text{CON}} = \sum_{i=1}^N \frac{1}{\text{Co}} \int_{\Omega} B(\phi_i) w(\phi_{\text{con}}) d\mathbf{x}, \quad (4)$$

with nondimensional capillary, interaction, and confinement number, Ca, In, and Co, respectively. The first is a Cahn-Hilliard energy, with $W(\phi_i) = \frac{1}{4}(\phi_i^2 - 1)^2$ a double-well potential and ϵ a small parameter determining the width of the diffuse interface. Due to this energy noninteracting cells tend to become circular. For simplicity, we here neglect other properties of the cell boundary, e.g., bending forces. In [30] they are shown to be negligible in the context of cell migration. The second is an interaction energy with $B(\phi_i) = (\phi_i + 1)/2$, a simple shift of ϕ_i to values in $[0, 1]$, and a cell-cell interaction potential,

$$w(\phi_j) = 1 - (a + 1) \left(\frac{\phi_j - 1}{2} \right)^2 + a \left(\frac{\phi_j - 1}{2} \right)^4, \quad (5)$$

approximating a short-range potential, which is only active within the interior of the cell and its diffuse boundary. The approach offers the possibility to consider repulsive as well as attractive interactions which can be tuned by parameter a (see Appendix A). The last energy models the interaction with the confinement, which is given by the phase field function $\phi_{\text{con}}(\mathbf{x}) = \tanh(\|\mathbf{x} - \mathbf{m}\| - r_{\text{con}})/(\sqrt{2}\epsilon)$, with $\mathbf{m} = (l/2, l/2)$ the center of the computational domain and

r_{con} the radius of the circular confinement. The interaction potential is the same as in Eq. (5), but we only consider repulsive interactions (see Appendix A).

For the definition of \mathbf{v}_i in Eq. (1), we follow the simplest possible approach, which can be considered as a generalization of active Brownian particles [32–34] to deformable objects [11]. In this approach the specified propulsion speed v_0 is the same for each cell, but the specified direction of motion, determined by the angle θ_i is controlled by rotational noise $d\theta_i(t) = \sqrt{2D_r} dW_i(t)$, with diffusivity D_r and a Wiener process W_i , which results in $\mathbf{v}_i = (\cos \theta_i, \sin \theta_i)$. Even if this mechanism of reorientation is the same for each cell, the outcome concerning shape and motion depends on the mechanical interaction considered through \mathcal{F}_{INT} and \mathcal{F}_{CON} . The growth rate k_i is sampled from a Gaussian distribution with mean and variance determined by the product of a constant growth factor k_{growth} and CIP factors for cell-cell interaction $f_i \in [0; 1]$ and cell-confinement interaction $\xi_i \in [0; 1]$, such that $k_i \sim N(f_i \xi_i k_{\text{growth}}, f_i \xi_i k_{\text{growth}})$. As a measure for contact, we consider the variational derivatives $\delta \mathcal{F}_{\text{INT}}/\delta \phi_i$ and $\delta \mathcal{F}_{\text{CON}}/\delta \phi_i$ and define the total interactions, $T_i = \int_{\Omega} \delta \mathcal{F}_{\text{INT}}/\delta \phi_i d\mathbf{x}$ and $T_{\text{con},i} = \int_{\Omega} \delta \mathcal{F}_{\text{CON}}/\delta \phi_i d\mathbf{x}$, which enter in

$$f_i = \max(0, \min(1 - \text{sgn}(T_i) \left(\frac{T_i}{L} \right)^2, 1)) \quad (6)$$

and ξ_i defined in the same way, with T_i replaced by $T_{\text{con},i}$. The parameter L is a limiting factor (see Appendix B). T_i/L and $T_{\text{con},i}/L$ are measures for mechanical interaction of cell ϕ_i with neighboring cells and the confinement, respectively. Considering the thermodynamically consistent definition for the cell pressure $P_i = \delta \mathcal{F}_{\text{INT}/\text{CON}}/\delta \phi_i$ and the associated passive stress $\sigma_i = -P_i \mathbb{I}$ (see [9]), these quantities provide a measure of the scalar average of the passive stress at cell ϕ_i .

Cell division is manually introduced if the cell size reaches a threshold. Following experimental evidence for epithelia tissue [35], we divide the cell perpendicular to its elongation axis. The number N of active cells is increased by one and the age of the two daughter cells start from zero. The overall size of the two daughter cells is slightly below that of the mother cell due to the necessity to introduce a diffuse interface between the two daughter cells. For further details, we refer to Appendix C.

III. NUMERICS AND PARAMETER SETTING

We employ a parallel and adaptive finite element method to solve the N coupled systems of partial differential equations for ϕ_i . The algorithm is implemented in AMDiS [36,37] and the algorithmic concepts to achieve parallel scaling with the number of cells N are described in [38]. Briefly, they consider one core for the evolution of each cell and parallel concepts from particle methods to reduce the communication overhead due to cell-cell interaction. The coupled fourth-order equations in Eq. (1) are split into coupled systems of second-order equations for the phase field variables ϕ_i and the corresponding chemical potentials $\mu_i = \delta \mathcal{F}/\delta \phi_i$. The discretization in time is semi-implicit with a Taylor expansion of the double-well potential and an explicit treatment of the other nonlinear terms. For the Cahn-Hilliard part we introduce

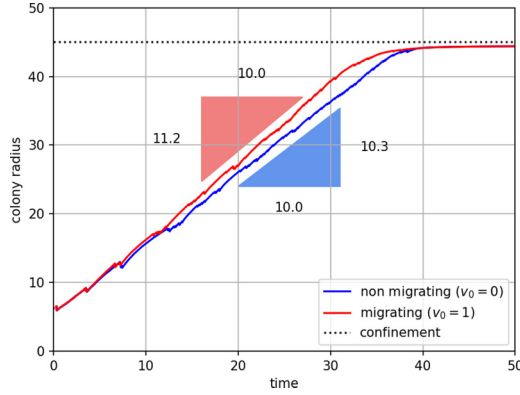


FIG. 2. Radius of a circle of corresponding area of growing colony over time and corresponding slope for $v_0 = \{0, 1\}$, $\text{In} = 0.05$, and $L = 10\,000$. The horizontal line shows the confinement, which is reached at $t \approx 40$. For related results with varying v_0 , In , and L see Appendix E.

an additional singular function in the energy (see [39]). This does not affect the asymptotic behavior as $\epsilon \rightarrow 0$ but helps to ensure $\phi_i \in [-1, 1]$ and to increase accuracy [40,41] (see Appendix D for details).

IV. RESULTS

We start with one circular cell, $N = 1$, in the center of a circular confinement within the computational domain, $\Omega = [0, l] \times [0, l]$. The size of the cell is just below the dividing threshold. Numerical parameters, such as grid resolution and time step are considered as large as possible to ensure stable behavior and resolution of the essential physics. The grid spacing within the diffuse boundary is $h \approx 0.2\epsilon$, in the interior of each cell $h \leq \epsilon$ and in the exterior $h \leq 10\epsilon$ with increasing values for regions far away from the interior. The time step is chosen as $\tau = 0.005$. Other parameters, if not specified differently, are set as $l = 100$, $r_{\text{con}} = 45$, $\epsilon = 0.15$, $\text{Ca} = 0.1$, $\text{Co} = 0.005$, $D_r = 0.01$, and $k_{\text{growth}} = 0.3$. We compare non-migrating and migrating cells ($v_0 = \{0, 1\}$) and consider $\text{In} = 0.05$ and $L = 10\,000$. Figure 2 shows the growth, expressed through the radius of a circle with the same area as the cell colony. The radius grows linearly and slightly faster for the migrating cells. This linear growth regime corresponds to a constant boundary velocity of the cell colony and is consistent with theoretical approaches, in which, due to CIP, only the cells at the boundary are able to grow and divide [25,28]. Exponential colony growth observed in early stages, e.g., in [24,25,28], is restricted to the growth of a single cell in our setting. Already for two cells, the deformability of the cells and the attachment forces lead to the emergence of a pronounced common edge, which restricts independent growth of the cells and thereby the linear growth regime kicks in earlier. In order to further analyze the effect of CIP on colony growth, we consider the age and the stress, expressed through T_i/L , of each cell (see Fig. 3). While for the nonmigrating case the age of the cells is more or less decreasing with increasing radius of the cell colony and the inner cells develop a homogeneous stress distribution, both age and stress are more heterogeneously distributed in the migrating case, which

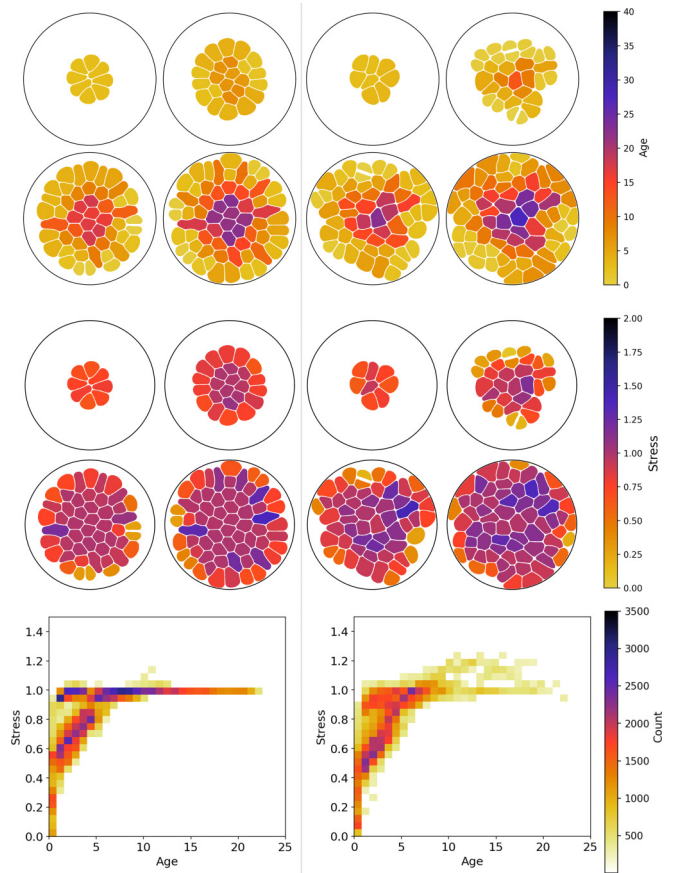


FIG. 3. Four snapshots of cell colony growth with color coding by age (top) and stress T_i/L (middle) for nonmigrating cells (left) and migrating cells (right). The corresponding times are $t = \{10, 20, 30, 35\}$. (Bottom) Corresponding relation between age and stress for all cells at all times $t \leq 35$. The color coding is with respect to the number of cells with the considered age/stress relation. Only points with more than 250 counts are shown.

is quantified in the age/stress diagrams. For cells with age below five, both diagrams are similar, indicating an increase of stress with age. But for cells with age above five, the diagrams differ. The homogeneous stress distribution for nonmigrating cells results in a horizontal line at $T_i/L \approx 1$. For migrating cells, this is less pronounced with larger stresses emerging, corresponding to a heterogeneous distribution. Therefore migrating cells can generate space, which allow them to grow further if the threshold for cell division is not reached. This increases the cell density and leads to stresses with $T_i/L > 1$.

The increased heterogeneity for the migrating case also becomes evident if the cell properties are averaged according to their position in the colony with respect to the center. Figure 4 shows the magnitude of the cell velocity and the measure for cell-cell interaction f_i . While the spatial-temporal distribution of the cell-cell interaction is similar for the non-migrating and migrating cases, the cell velocities strongly differ. Not only within the center of the colony, where the nonmigrating cells are more or less stationary and significant movement is present for the migrating cells, but also on the colony boundary, which shows significantly larger velocities for the migrating cells. It has been argued that this larger

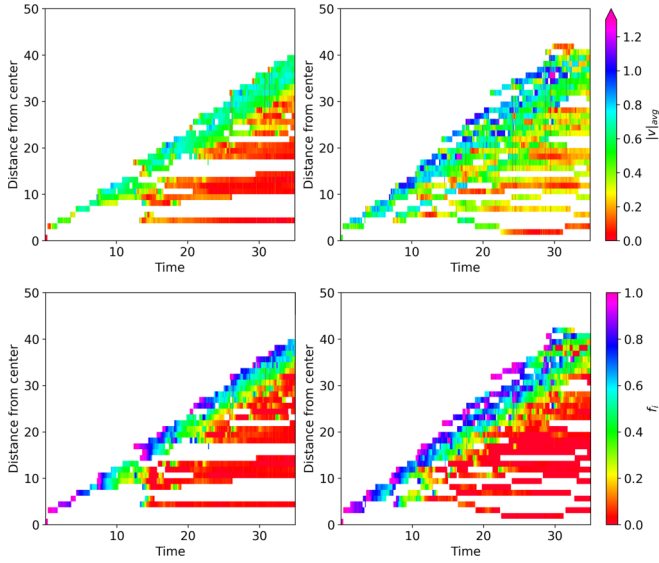


FIG. 4. Radial analysis. (Top) Magnitude of cell velocity $|\mathbf{v}|_{\text{avg}}$ as a function of distance from colony center and time. (Bottom) Measure of cell-cell interaction f_i . (Left) nonmigrating; (right) migrating cells.

velocity at the colony boundary is the main reason for the increased growth rate in the migrating case and that at long times the colony expands as fast as the cells on the boundary are able to migrate away from the colony center. This relation between the strength of activity and the growth rate of the colony is consistent within the considered parameter range (see Appendix E). The colony grows faster for larger values of v_0 .

Another measure concerns the topology of the cells in the colony. We consider the coordination number, the number of nearest neighbors, for each cell and calculate the histogram (see Fig. 5). The data is shown for different time instances. On average, the number of neighbors evolves similarly for the nonmigrating and the migrating cells [see Fig. 5 (right)], and reaches six, which is consistent with Euler’s polyhedral formula. However, the histograms show the difference between the nonmigrating and migrating cases [see Fig. 5 (left, middle)]. While for nonmigrating cells a steady-state configuration emerges, with a strong peak at six neighbors, the structure of the migrating cells is more heterogeneous with

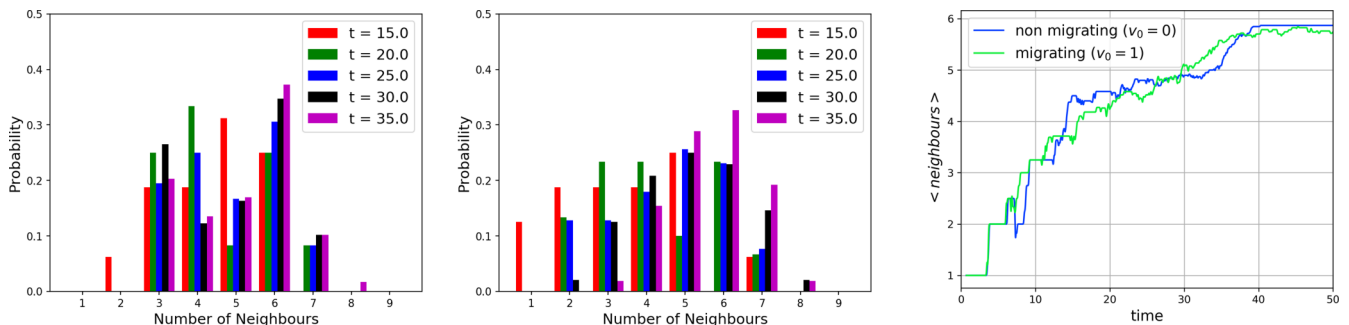


FIG. 5. Histogram of the coordination number of the cells at different times: (left) nonmigrating, (middle) migrating cells. (Right) Averaged number of neighbors over time for both cases. Only the cells not touching the confinement are considered.

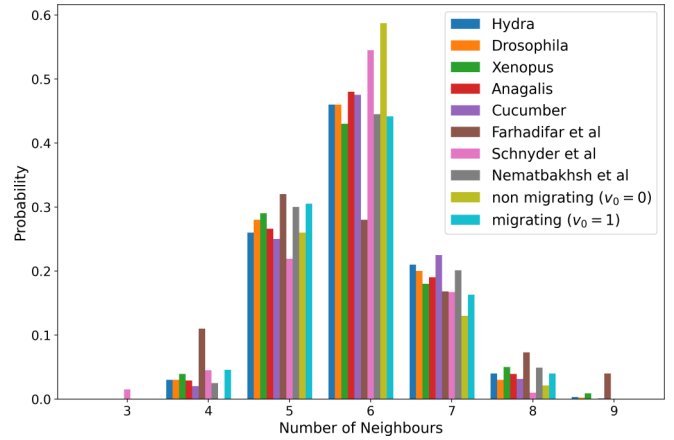


FIG. 6. Experimental coordination number reported in the literature: *Drosophila*, *Xenopus*, *Hydra* [42], *Anagallis*, cucumber [43], together with computational results [28,44,45] and our migrating ($v_0 = 1$) and nonmigrating ($v_0 = 0$) results for $t > 50$.

significantly more cells with five and seven neighbors. For tissues where cell proliferation is the primary cell activity, measurements on embryonic epithelial tissues have shown that the statistics of the coordination numbers are universal [42]. Figure 6 shows experimental data together with various simulation approaches and our results. As most of the experimental data are for cells in confinements, we consider the late time behavior for $t > 50$ and show the average of the distribution over time. While the nonmigrating case overestimates the number of cells with six neighbors, the migrating case is in reasonable agreement with the experimental data and other simulation approaches.

V. CONCLUSIONS

In summary, we have used a multiphase field model to explore the effect of CIP in growing colonies of nonmigrating and migrating cells. The extension of the multiphase field model, as a minimal cell-based model, which accounts for cell deformability and force transmission at cell-cell contacts, to growth and cell division, allows one to analyze the impact of contact inhibition. CIP is included by linking cellular growth to the short-range interaction with neighboring cells, which is realized by considering the chemical potential associated

with the interaction energies. The stochastic behavior of migration and growth on a single cell level manifests in global patterns in a multicellular context. The emerging neighbor distribution in the growing colony is a result of cell division. Under the influence of confinement it is in good agreement with experimental measurements for various organisms. The agreement for the migrating case is better; the nonmigrating case overestimates the number of cells with six neighbors. The proposed model leads to the typical linear boundary growth of the colony radius with increased growth rate for increased activity. It further allows for various investigations concerning cell velocity, age, and stress distributions. They all significantly differ between nonmigrating and migrating cells and ask for experimental validations.

ACKNOWLEDGMENTS

A.V. acknowledges support by the German Research Foundation (DFG) under Grant No. FOR3013. We further acknowledge computing resources provided at Jülich Supercomputing Center under Grant No. PFAMDIS.

APPENDIX A: INTERACTION POTENTIAL

To compute the interaction between two deformable objects typically requires nonlocal terms. Here, this is circumvented by considering the phase field variables of all cells. The term $B(\phi_i) \sum_{j \neq i} w(\phi_j)$ in \mathcal{F}_{INT} considers the interactions of cell i with all other cells. The short-range nature of the interaction results from $B(\phi_i)$, which is nonzero only at the interior of the cell and within its diffuse boundary. Figure 7 shows the impact of the parameter a in the definition of w in Eq. (5) in the main text and the considered strength of interaction between two cells for $a = 1.5$ (attractive and repulsive) and $a = 1$ (repulsive), to be used for \mathcal{F}_{INT} and \mathcal{F}_{CON} , respectively. Figure 7 also shows the interaction potential ω as a function of the signed distance d of the $\phi = 0$ level set, which can be computed from the equilibrium \tanh profile of the phase field $\phi = \tanh(d(\mathbf{x}, t)/(\sqrt{2}\epsilon))$ (see [18,46]):

$$d = -\frac{\epsilon}{\sqrt{2}} \ln \left(\frac{1 + \phi}{1 - \phi} \right). \tag{A1}$$

This only holds within the diffuse interface $-1 < \phi < 1$. Negative values correspond to the interior of the cell.

APPENDIX B: MODELING CIP

Influencing the growth rate k_i solely by the chemical potentials, which are associated with the interaction and confinement energies, \mathcal{F}_{INT} and \mathcal{F}_{CON} , respectively, provides a way to measure contact without any additional computations. The considered functional form for f_i and ξ_i (see Fig. 8) provides one possibility to have unlimited growth for total interaction $T_i \leq 0$, and a nonlinear reduction towards suppressed growth if $T_i \leq L$, with adjustable parameter L . T_i/L is used as a measure of stress in the modeling approach for CIP.

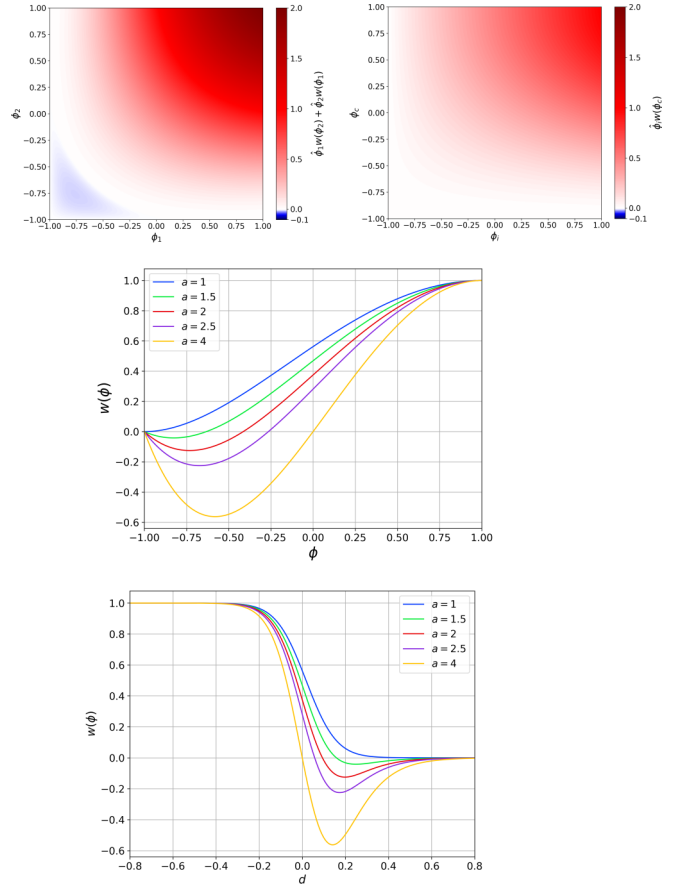


FIG. 7. (Top) The considered interaction energies for cell-cell interaction, $a = 1.5$ (attractive and repulsive, left) and cell-confinement interaction, $a = 1$ (repulsive, right). (Middle and bottom) Functional form for the interaction potential for different parameters a as a function of phase field ϕ and signed distance d from the $\phi = 0$ level set.

APPENDIX C: CELL DIVISION

Cell division depends on cell size and cell geometry. Cell area/volume is easily measured as $V_i = \int_{\Omega} B(\phi_i) d\mathbf{x}$. In order to find the elongation axis we compute the Q tensor (symmetric and trace-free tensor) for the cells which are above a given

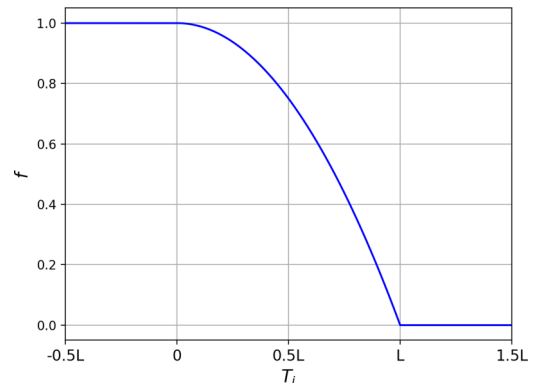


FIG. 8. CIP factor f_i for cell-cell interaction. The CIP factor ξ_i for cell-confinement interaction has the same functional form.

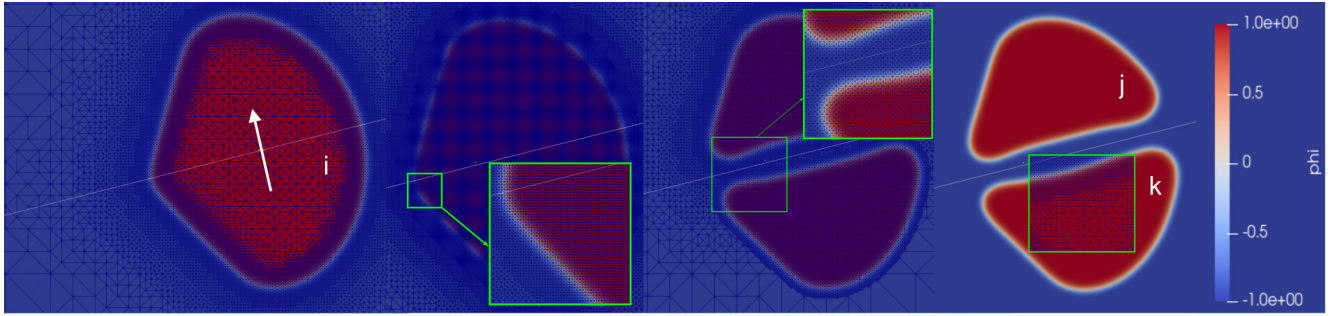


FIG. 9. (From left to right) Phase field ϕ_i of a cell along with the mesh. If the volume of the cell reaches the threshold for division the \mathbf{Q} tensor \mathbf{S}_i is computed. The white arrow marks the largest eigenvector of \mathbf{S}_i , and the white line, perpendicular to the vector, is the axis along which the cell will divide. Next, the mesh is refined within the cell. Then, the cell is divided along the specified axis by setting $\phi_i = -1$ within a small band along the dividing axis. New indices j and k are assigned to the phase fields of the daughter cells. The fine mesh guarantees recovering the characteristic tanh profile within one time step. Last, the new phase fields ϕ_j and ϕ_k along with the coarsened mesh after 10 time steps after the division.

threshold for V_i . This reads

$$\mathbf{S}_i = \int \begin{bmatrix} \frac{1}{2}((\partial_y \phi_i)^2 - (\partial_x \phi_i)^2) & -(\partial_x \phi_i)(\partial_y \phi_i) \\ -(\partial_x \phi_i)(\partial_y \phi_i) & \frac{1}{2}((\partial_x \phi_i)^2 - (\partial_y \phi_i)^2) \end{bmatrix} d\mathbf{x}.$$

The eigenvector of \mathbf{S}_i corresponding to the largest eigenvalue points along the elongation axis of the cell. The cell is divided perpendicular to this axis by assigning $\phi_i = -1$ along a small strip passing through the center of mass, defined as $\mathbf{c}_i = (\int_{\Omega} B(\phi_i) \mathbf{x} d\mathbf{x}) / (\int_{\Omega} B(\phi_i) d\mathbf{x})$. The width of this strip is considered to be of order ϵ . Two new phase fields are assigned

according to the proposed approach in [4]. Resulting sharp corners are smeared out in the next time step due to \mathcal{F}_{CH} and also the slight loss of area/volume is compensated within the next time steps due to growth. Numerically we also refine the mesh before cell division and coarsen the mesh after cell division. The grid spacing for the interior of the cell to be divided corresponds to that of the diffuse boundary, $h \approx 0.2\epsilon$. This certainly increases the computational cost, but it only happens localized in space (restricted to $\phi_i = 1$) and time (within a few time steps). Figure 9 shows an example of a cell division process.

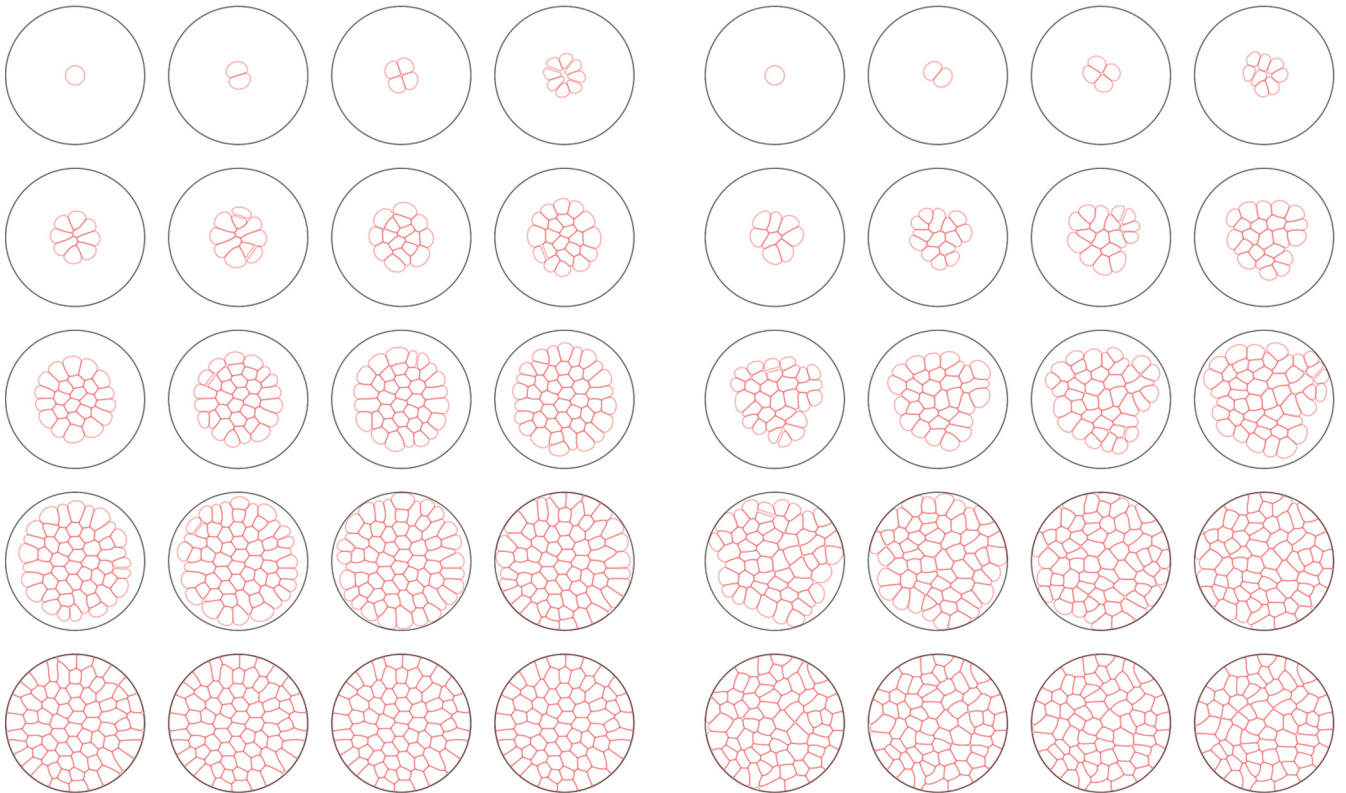


FIG. 10. Snapshots of colony growth. (Left) Nonmigrating, (right) migrating cells. The time instances are $\{0, 2.5, 5, 7.5, 10, 12.5, 15, 17.5, 20, 22.5, 25, 27.5, 30, 32.5, 35, 37.5, 40, 42.5, 45, 47.5\}$. All postprocessing concerning colony growth is limited to $t \leq 35$ to exclude the influence of the confinement. The corresponding movies are provided in the Supplemental Material [29].

APPENDIX D: NUMERICAL STABILISATION

Following [39] we use instead of the Cahn-Hilliard energy,

$$\mathcal{F}_{CH} = \sum_{i=1}^N \frac{1}{Ca} \int_{\Omega} \frac{\epsilon}{2} \|\nabla \phi_i\|^2 + \frac{1}{\epsilon} W(\phi_i) d\mathbf{x},$$

a degenerate form,

$$\mathcal{F}_{DCH} = \sum_{i=1}^N \frac{1}{Ca} \int_{\Omega} g_{\alpha}(\phi_i) \left(\frac{\epsilon}{2} \|\nabla x s \phi_i\|^2 + \frac{1}{\epsilon} W(\phi_i) \right) d\mathbf{x},$$

with

$$g_{\alpha}(\phi_i) = \frac{1}{\sqrt{\gamma^2(\phi_i + 1)^2(\phi_i - 1)^2 + \alpha^2 \epsilon^2}}, \quad \gamma > 0, \alpha > 0,$$

with appropriate γ to ensure scaling properties and α to guarantee differentiability. This modification does not affect the asymptotic behavior as $\epsilon \rightarrow 0$ but helps to ensure $\phi_i \in [-1, 1]$ and to increase accuracy (see [39,41]).

APPENDIX E: ADDITIONAL RESULTS

Figure 10 shows snapshots of all cells in the colony corresponding to Fig. 1 in the main text. Besides the different morphologies of the colony boundary also the stronger deformations of the individual cells for migrating cells are visible. Only configurations with $t \leq 35$ are considered in any post-processing concerning colony growth to exclude the influence of the confinement.

In order to demonstrate the differences in colony growth between nonmigrating and migrating cells we consider the results of Fig. 2 in the main text for different parameters In and L . Figure 11 shows the corresponding behavior and the robustness of the qualitative differences, showing faster colony boundary growth for migrating cells.

We further vary v_0 . Figure 12 shows the corresponding results to Fig. 2 in the main text for various v_0 . The results confirm the linear colony growth with a growth rate which is proportional to v_0 . However, this trend reverses as soon as

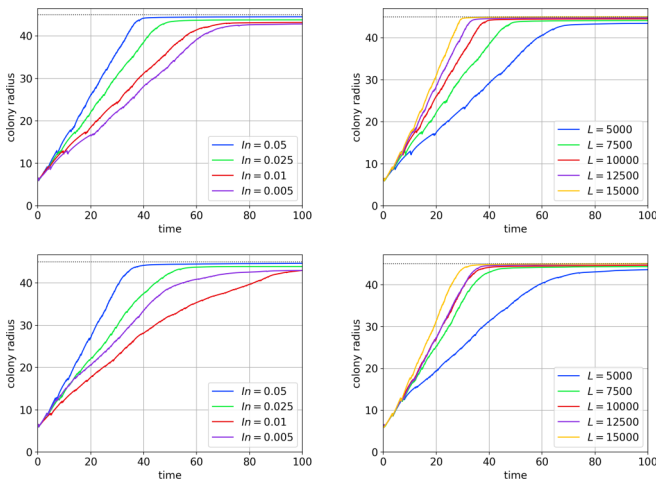


FIG. 11. Evolution of colony radius for nonmigrating cell (top) and migrating cells (bottom) for different values of In and L with $L = 10\,000$ (left) and $In = 0.05$ (right).

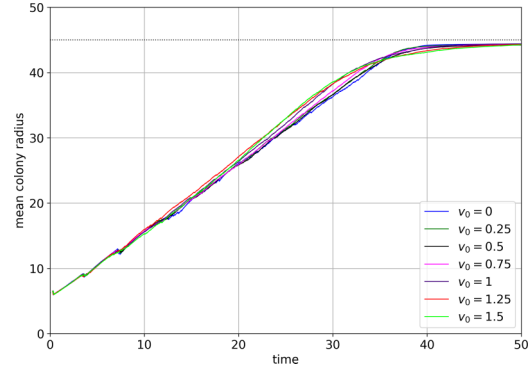


FIG. 12. Evolution of colony radius for different v_0 with $L = 10\,000$ and $In = 0.05$.

the colony gets in contact with the confinement. As colonies of migrating cells reach the confinement faster the additional effects of CIP due to the interaction with the confinement slow down the growth of the colony from this time on.

As a last example we consider the late time behavior, for which the influence of the confinement becomes significant. Figure 13 shows the resulting configurations varying L , In , and v_0 . Increasing L reduces the measures for stress T_i/L and $T_{con,i}/L$ and thus also the effect of CIP. This leads to faster growth of the cells and within the confinement to larger packing fractions and more polygonal cell shapes.

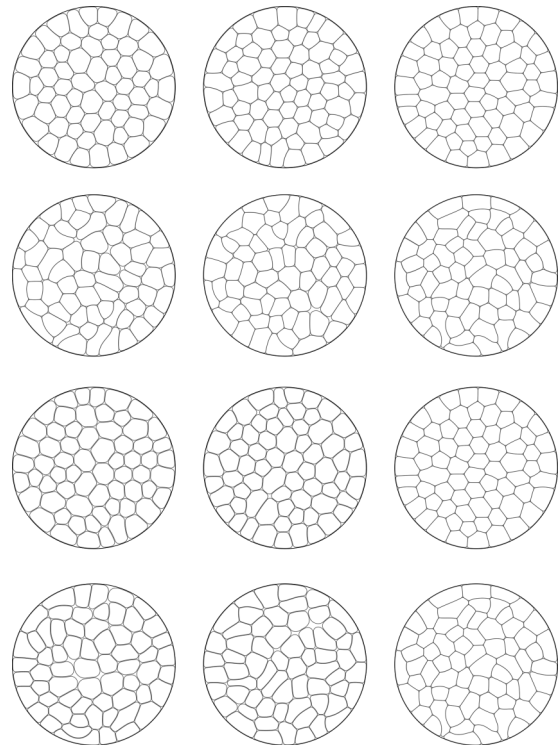


FIG. 13. Colony snapshots at late times after the confinement is filled. (Row 1) $L = 5000, 7500$, and $10\,000$ (left to right) for $In = 0.05$ and $v_0 = 0$. (Row 2) $L = 5000, 7500$, and $10\,000$ (left to right) for $In = 0.05$ and $v_0 = 1$. (Row 3) $In = 0.005, 0.01$, and 0.05 (left to right) for $L = 10\,000$ and $v_0 = 0$. (Row 4) $In = 0.005, 0.01$, and 0.05 (left to right) for $L = 10\,000$ and $v_0 = 1$.

The remaining free space and roundish cells in contrast to the tightly packed and polygonal cells are clearly visible in the first row, which considers the nonmigrating case. This behavior qualitatively remains for the migrating case (see second row). However, the cell configurations are more heterogeneous, with respect to size, cell shape, and number of

neighbors for the migrating case. This is consistent with the observations in the growing colony (see Fig. 10). Similar results are obtained if In is increased. This decreases \mathcal{F}_{INT} and therefore T_i and thus leads to a similar effect, as seen in the third and fourth row, for nonmigrating and migrating cells, respectively.

- [1] V. Hakim and P. Silberzan, Collective cell migration: a physics perspective, *Rep. Prog. Phys.* **80**, 076601 (2017).
- [2] R. Alert and X. Trepat, Physical models of collective cell migration, *Ann. Rev. Cond. Matt. Phys.* **11**, 77 (2020).
- [3] A. Moure and H. Gomez, Phase-field modeling of individual and collective cell migration, *Arch. Comput. Meth. Eng.* **28**, 311 (2021).
- [4] M. Nonomura, Study on multicellular systems using a phase field model, *PLoS ONE* **7**, e33501 (2012).
- [5] B. A. Camley, Y. Zhang, Y. Zhao, B. Li, E. Ben-Jacob, H. Levine, and W.-J. Rappel, Polarity mechanisms such as contact inhibition of locomotion regulate persistent rotational motion of mammalian cells on micropatterns, *Proc. Nat. Acad. Sci. USA* **111**, 14770 (2014).
- [6] J. Loeber, F. Ziebert, and I. S. Aranson, Collisions of deformable cells lead to collective migration, *Sci. Rep.* **5**, 9172 (2015).
- [7] B. Palmieri, Y. Bresler, D. Wirtz, and M. Grant, Multiple scale model for cell migration in monolayers: Elastic mismatch between cells enhances motility, *Sci. Rep.* **5**, 11745 (2015).
- [8] D. A. Kulaviak, B. A. Camlay, and W.-J. Rappel, Modeling contact inhibition of locomotion of colliding cells migrating on micropatterned substrates, *PLoS Comput. Biol.* **12**, e1005239 (2016).
- [9] R. Mueller, J. M. Yeomans, and A. Doostmohammadi, Emergence of Active Nematic Behavior in Monolayers of Isotropic Cells, *Phys. Rev. Lett.* **122**, 048004 (2019).
- [10] D. Wenzel, S. Praetorius, and A. Voigt, Topological and geometrical quantities in active cellular structures, *J. Chem. Phys.* **150**, 164108 (2019).
- [11] B. Loewe, M. Chiang, D. Marenduzzo, and M. C. Marchetti, Solid-Liquid Transition of Deformable and Overlapping Active Particles, *Phys. Rev. Lett.* **125**, 038003 (2020).
- [12] D. Wenzel and A. Voigt, Multiphase field models for collective cell migration, *Phys. Rev. E* **104**, 054410 (2021).
- [13] G. Peyret, R. Mueller, J. d'Alessandro, S. Begnaud, P. Marcq, R.-M. Mege, J. M. Yeomans, A. Doostmohammadi, and B. Ladoux, Sustained oscillations of epithelial cell sheets, *Biophys. J.* **117**, 464 (2019).
- [14] L. Balasubramaniam, A. Doostmohammadi, T. B. Saw, G. H. N. S. Narayana, R. Mueller, T. Dang, M. Thomas, S. Gupta, S. Sonam, A. S. Yap, Y. Toyama, R.-M. Mége, J. M. Yeomans, and B. Ladoux, Investigating the nature of active forces in tissues reveals how contractile cells can form extensile monolayers, *Nat. Mater.* **20**, 1156 (2021).
- [15] B. Stramer and R. Mayor, Mechanisms and in vivo functions of contact inhibition of locomotion, *Nature Rev. Mol. Cell Bio.* **18**, 43 (2017).
- [16] H. W. Fisher and J. Yeh, Contact inhibition in colony formation, *Science* **155**, 581 (1967).
- [17] M. G. P. Stoker and H. Rubin, Density dependent inhibition of cell growth in culture, *Nature (London)* **215**, 171 (1967).
- [18] W. Marth and A. Voigt, Collective migration under hydrodynamic interactions: a computational approach, *Interf. Focus* **6**, 20160037 (2016).
- [19] S. Najem and M. Grant, Phase-field model for collective cell migration, *Phys. Rev. E* **93**, 052405 (2016).
- [20] D. Zwicker, R. Seyboldt, C. A. Weber, A. A. Hyman, and F. Juelicher, Growth and division of active droplets provides a model for protocells, *Nature Physics* **13**, 408 (2017).
- [21] I. Y. Li and M. E. Cates, Non-equilibrium phase separation with reactions: a canonical model and its behaviour, *J. Stat. Mech.* (2020) 053206.
- [22] D. Drasdo, R. Kree, and J. S. McCaskill, Monte-Carlo approach to tissue-cell populations, *Phys. Rev. E* **52**, 6635 (1995).
- [23] M. Basan, J. Elgeti, E. Hannezo, W.-J. Rappel, and H. Levine, Alignment of cellular motility forces with tissue flow as a mechanism for efficient wound healing, *Proc. Nat. Acad. Sci. USA* **110**, 2452 (2013).
- [24] S. Aland, H. Hatzikirou, J. Lowengrub, and A. Voigt, A mechanistic collective cell model for epithelial colony growth and contact inhibition, *Biophys. J.* **109**, 1347 (2015).
- [25] A. Puliafito, L. Hufnagel, P. Neveu, S. Streichan, A. Sigal, D. K. Fygenson, and B. I. Shraiman, Collective and single cell behavior in epithelial contact inhibition, *Proc. Nat. Acad. Sci. USA* **109**, 739 (2012).
- [26] K. Doxzen, S. R. K. Vedula, M. C. Leong, H. Hirata, N. S. Gov, A. J. Kabla, B. Ladoux, and C. T. Lim, Guidance of collective cell migration by substrate geometry, *Integ. Bio.* **5**, 1026 (2013).
- [27] M. George, F. Bullo, and O. Campas, Connecting individual to collective cell migration, *Sci. Rep.* **7**, 9720 (2017).
- [28] S. K. Schnyder, J. J. Molina, and R. Yamamoto, Control of cell colony growth by contact inhibition, *Sci. Rep.* **10**, 6713 (2020).
- [29] See Supplemental Material at <http://link.aps.org/supplemental/10.1103/PhysRevE.105.034402> for corresponding movies.
- [30] W. Marth, S. Praetorius, and A. Voigt, A mechanism for cell motility by active polar gels, *J. Roy. Soc. Interf.* **12**, 20150161 (2015).
- [31] D. Wenzel, M. Nestler, S. Reuther, M. Simon, and A. Voigt, Defects in active nematics - algorithms for identification and tracking, *Comput. Meth. Appl. Math.* **21**, 683 (2021).
- [32] Y. Fily and M. C. Marchetti, Athermal Phase Separation of Self-Propelled Particles with no Alignment, *Phys. Rev. Lett.* **108**, 235702 (2012).
- [33] G. S. Redner, A. Baskaran, and M. F. Hagan, Reentrant phase behavior in active colloids with attraction, *Phys. Rev. E* **88**, 012305 (2013).
- [34] A. Wysocki, R. G. Winkler, and G. Gompper, Cooperative motion of active Brownian spheres in three-dimensional dense suspensions, *EPL* **105**, 48004 (2014).
- [35] T. P. J. Wyatt, A. R. Harris, M. Lam, Q. Cheng, J. Bellis, A. Dimitracopoulos, A. J. Kabla, G. T. Charras, and B. Baum,

- Emergence of homeostatic epithelial packing and stress dissipation through divisions oriented along the long cell axis, *Proc. Nat. Acad. Sci. USA* **112**, 5726 (2015).
- [36] S. Vey and A. Voigt, AMDiS: Adaptive multidimensional simulations, *Comput. Vis. Sci.* **10**, 57 (2007).
- [37] T. Witkowski, S. Ling, S. Praetorius, and A. Voigt, Software concepts and numerical algorithms for a scalable adaptive parallel finite element method, *Adv. Comput. Math.* **41**, 1145 (2015).
- [38] S. Praetorius and A. Voigt, Collective cell behavior - a cell-based parallelization approach for a phase field active polar gel model, in *NIC Symposium 2018*, edited by K. Binder, M. Müller, and A. Trautmann (Forschungszentrum Jülich GmbH, Jülich, 2018), pp. 369–376.
- [39] M. Salvalaglio, A. Voigt, and S. M. Wise, Doubly degenerate diffuse interface models of surface diffusion, *Math. Meth. Appl. Sci.* **44**, 5385 (2021).
- [40] A. Rätz, A. Ribalta, and A. Voigt, Surface evolution of elastically stressed films under deposition by a diffuse interface model, *J. Comput. Phys.* **214**, 187 (2006).
- [41] R. Backofen, S. M. Wise, M. Salvalaglio, and A. Voigt, Convexity splitting in a phase field model for surface diffusion, *Int. J. Math. Anal. Mod.* **16**, 192 (2019).
- [42] M. C. Gibson, A. B. Patel, R. Nagpal, and N. Perrimon, The emergence of geometric order in proliferating metazoan epithelia, *Nature (London)* **442**, 1038 (2006).
- [43] A. B. Patel, W. T. Gibson, M. C. Gibson, and R. Nagpal, Modeling and inferring cleavage patterns in proliferating epithelia, *PLoS Comput. Biol.* **5**, e1000412 (2009).
- [44] R. Farhadifar, J.-C. Roper, B. Algouy, S. Eaton, and F. Jülicher, The influence of cell mechanics, cell-cell interactions, and proliferation on epithelial packing, *Curr. Biol.* **17**, 2095 (2007).
- [45] A. Nematbakhsh, W. Sun, P. A. Brodskiy, A. Amiri, C. Narciso, Z. Xu, J. J. Zartman, and M. Alber, Multi-scale computational study of the mechanical regulation of cell mitotic rounding in epithelia, *PLoS Comput. Biol.* **13**, e1005533 (2017).
- [46] W. Marth, S. Aland, and A. Voigt, Margination of white blood cells: a computational approach by a hydrodynamic phase field model, *J. Fluid Mech.* **790**, 389 (2016).